Return to Session Directory

DYNAMIC POSITIONING CONFERENCE
October 15-16, 2013

RISK SESSION

Cooperative Control Applied to Multi-Vessel DP Operations - Numerical and Experimental Analysis

By Asdrubal N. Queiroz Filho and Eduardo A. Tannuri

University of São Paulo, Numerical Offshore Tank, TPN-USP

Abstract

Offshore operations involving several floating units are becoming more frequent nowadays. Such operations are used for sub-sea equipment installation for example. This kind of operations requires a high level of coordination between the vessels, which today is made without the ship's information exchange, being each ship individually commanded. Therefore, in those cases, a cooperative control could be applied, ensuring that the relative distance between the ships are maintained in a limited range, controlling operational parameters such as the lifting line traction. The benefits of this control are shown when compared to the non cooperative control by means of an experimental set-up with two DP vessels and numerical simulations.

Introduction

Nowadays with the increasing of ultra-deep water oil & gas exploration a new concept of "platform" is rising, where all extracting equipment is placed at the sea's bottom. This new concept is already used in some fields around the world as in Ormen Lange in Norway (Fig. 1) and has proved to be economically viable.

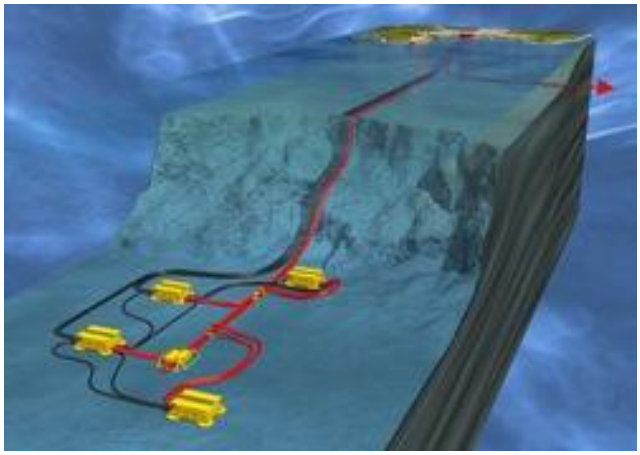

Fig. 1. Gas explorations field in Ormen Lange Norway.

Since they are normally large and requires a precise positioning in the sea floor, the installation requires multi-vessels operations. Those operations require a high level of planning and coordination. An example that involves the operation of two ships was studied by Fujarra et al. (2008). Multi-vessels operations are cases where cooperative control could be applied.

Considering the oil & gas industry, there are many other cases where cooperative control could be applied. In Queiroz et. al. (2012) an oil transfer operation was studied. Two shuttle tankers had to maintain their relative position while oil was transferred between them, in order to avoid the necessity of shore terminals. A fully numerical time domain simulation was carried on and the results showed the benefits of the cooperative control, when compared to the non-cooperative one. In that paper, the cooperative controller was designed using LQG-LTR control theory applied to the multivariable system model involving the states of both vessels.

Back to sub-sea equipment installation, it is important to coordinate the relative movement between the ships in order to properly place the equipment or structure at the sea bottom. This case will be evaluated in the present paper considering a conceptual experiment.

The cooperative DP controller will be deeper investigated with the analysis of the coupled dynamics of the vessels. The influence of the cooperative control gains will be discussed, using the frequency response and the pole-placement analysis. The consensus control concepts are applied, following Ren et al. (2007). The advantage of the cooperative control is demonstrated, with the reduction of the relative positioning error during station keeping or transient manoeuvres.

Fully nonlinear time-domain simulations and a small-scale experiment will be used to demonstrate the advantages of the cooperative control. All tests are carried out using the TPN's numerical simulator (as described in Nishimoto et al. 2003) and TPN's physical tank. Two small-scale offshore tugboats models are used for the scale experiment. Both of them are equipped with two main thrusters at the ship's stern, two tunnel thrusters, one in the bow and one in the stern.

Mathematical Modeling

The DP System is only concerned about the horizontal motions of the vessel, that is, surge, sway and yaw. The motions of the vessels are expressed in two separate coordinate systems (Fig 2): one is the inertial system fixed to the Earth, OXYZ (also known as global reference system); and the other, Ax_1^A x_2^A x_6^A or Bx_1^B x_2^B x_6^B, are the vessel-fixed non-inertial reference frames (also known as local reference system). The origin for this system is the intersection of the amidships section with the ship's longitudinal plane of symmetry. The axes for this system coincide with the principal axes of inertia of the vessel with respect to the origin. The motions along the local axis are called surge, sway e yaw, respectively.

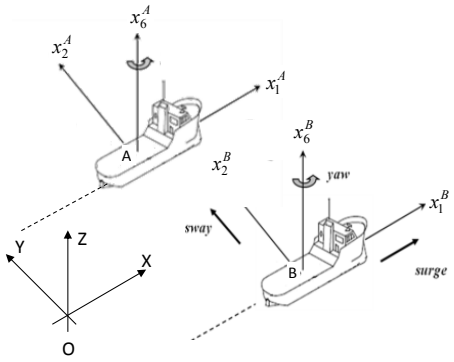

Fig. 2. Coordinate systems.

Considering the two ships to be parallel to each other, with their local reference system aligned to the global reference system, small yaw rotation angles (smaller than 10°) and disregarding non-linear dynamics and damping terms the simplified systems' dynamics horizontal motion with respect to the global reference system are given by:

$$\left(\boldsymbol{M}_A + \boldsymbol{M}_A^{ad}\right)\ddot{\boldsymbol{x}}_A + \boldsymbol{D}_A\dot{\boldsymbol{x}}_A = \boldsymbol{u}_A + \boldsymbol{F}_A^d \qquad (1)$$

$$\left(\boldsymbol{M}_B + \boldsymbol{M}_B^{ad}\right)\ddot{\boldsymbol{x}}_B + \boldsymbol{D}_B\dot{\boldsymbol{x}}_B = \boldsymbol{u}_B + \boldsymbol{F}_B^d \qquad (2)$$

where index A and B refer to vessel A and B and the vectors $\boldsymbol{x}_{A,B}$ are given by $\boldsymbol{x}_{A,B} = \left[\boldsymbol{x}_1^{A,B} \quad \boldsymbol{x}_2^{A,B} \quad \boldsymbol{x}_6^{A,B}\right]^T$ is the position of the local reference system of each ship with respect to the global one.

The system's parameters values and a short description can be found in Table 1.

Table 1. System's parameters description.

Parameter	Description
$\boldsymbol{M_{A,B}}$	Vessel's horizontal displacement matrix
$\boldsymbol{M_{A,B}^{ad}}$	Vessel's added mass matrix
$\boldsymbol{D}_{\mathrm{A,B}}$	Vessel's linear damping matrix
$\boldsymbol{u}_{\mathrm{A,B}}$	Vessel's horizontal DP force vector
$\boldsymbol{F_{A,B}^{d}}$	Vessel's horizontal disturbance force caused by environmental agents

The dynamics of the relative motion can be obtained by eqs. (1) - (2):

$$\left(\boldsymbol{M_A} + \boldsymbol{M_A^{ad}} - \boldsymbol{M_B} - \boldsymbol{M_B^{ad}}\right)\ddot{\boldsymbol{x}}_A + (\boldsymbol{M_B} + \boldsymbol{M_B^{ad}})(\ddot{\boldsymbol{x}}_A - \ddot{\boldsymbol{x}}_B) + (\boldsymbol{D_A} - \boldsymbol{D_B})\dot{\boldsymbol{x}}_A + \boldsymbol{D_B}(\dot{\boldsymbol{x}}_A - \dot{\boldsymbol{x}}_B) = \boldsymbol{u_A} - \boldsymbol{u_B} + \boldsymbol{F_A^d} - \boldsymbol{F_B^d} \quad (3)$$

Defining the relative position as $\Delta\boldsymbol{x} \triangleq \boldsymbol{x_A} - \boldsymbol{x_B}$ and $\Delta\boldsymbol{F^d} \triangleq \boldsymbol{F_A^d} - \boldsymbol{F_B^d}$ as the difference of disturbance forces action on the vessels, the dynamics of the relative motion can be obtained as follows:

$$(\boldsymbol{M_A} + \boldsymbol{M_A^{ad}} - \boldsymbol{M_B} - \boldsymbol{M_B^{ad}})\ddot{\boldsymbol{x}}_A + (\boldsymbol{M_B} + \boldsymbol{M_B^{ad}})\Delta\ddot{\boldsymbol{x}} + (\boldsymbol{D_A} - \boldsymbol{D_B})\dot{\boldsymbol{x}}_A + \boldsymbol{D_B}\Delta\dot{\boldsymbol{x}} = \boldsymbol{u_A} - \boldsymbol{u_B} + \Delta\boldsymbol{F^d} \quad (4)$$

If the two ships are considered to have the same parameters ($\boldsymbol{M_A} = \boldsymbol{M_B} = \boldsymbol{M}$; $\boldsymbol{M_A^{ad}} = \boldsymbol{M_A^{ad}} = \boldsymbol{M^{ad}}$; $\boldsymbol{D_A} = \boldsymbol{D_B} = \boldsymbol{D}$), eq. (4) can be simplified as:

$$\left(\boldsymbol{M} + \boldsymbol{M^{ad}}\right)\Delta\ddot{\boldsymbol{x}} + \boldsymbol{D}\Delta\dot{\boldsymbol{x}} = \boldsymbol{u_A} - \boldsymbol{u_B} + \Delta\boldsymbol{F^d} \quad (5)$$

The non cooperative control model

The non cooperative control model is given by 3-uncoupled PID controllers for each vessel. Fig. 3 shows the control layout.

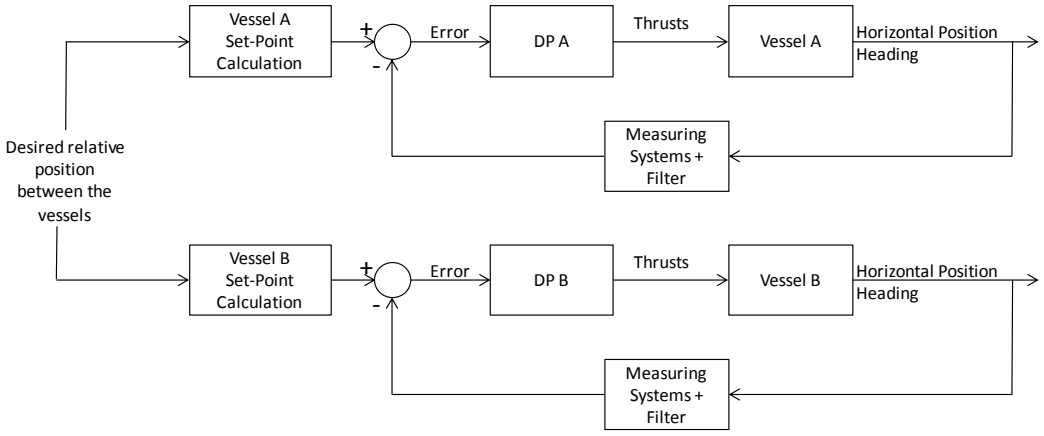

Fig. 3. Non cooperative control system.

Considering that the two vessels are similar, the same control gains are used. The control law $\boldsymbol{u_{A,B}}$ are then given by:

$$\boldsymbol{u_{A,B}} = \boldsymbol{K_P e_{A,B}} + \boldsymbol{K_D}\dot{\boldsymbol{e}}_{\boldsymbol{A,B}} + \boldsymbol{K_I}\int \boldsymbol{e_{A,B}}dt \quad (6)$$

where $\boldsymbol{e}_{A,B}$ refers to the position error signal (error in Fig. 3). The $\boldsymbol{K}_P$, $\boldsymbol{K}_D$ and $\boldsymbol{K}_I$ refers to the PID's proportional, derivative and integrative diagonal gains matrixes respectively. Replacing eq. (6) in eq. (5) the non cooperative closed-loop system stays as:

$$\left(\boldsymbol{M}+\boldsymbol{M}^{ad}\right)\Delta\ddot{\boldsymbol{x}}+(\boldsymbol{D}+\boldsymbol{K}_D)\Delta\ddot{\boldsymbol{x}}+\boldsymbol{K}_P\Delta\dot{\boldsymbol{x}}+\boldsymbol{K}_I\Delta\boldsymbol{x}=\boldsymbol{K}_D\Delta\ddot{\boldsymbol{r}}+\boldsymbol{K}_P\Delta\dot{\boldsymbol{r}}+\boldsymbol{K}_I\Delta\boldsymbol{r}+\Delta\boldsymbol{F}^d \quad (7)$$

where $\Delta\boldsymbol{r}$ is the desired relative position between the vessels (relative position set-point).

The cooperative control model

The cooperative control model combines the existent DP system of each vessel with the consensus concepts, presented by Ren et al. (2007). In this paper, only a "proportional" consensus gain will be adopted. Fig. 4 shows the controller layout.

Again the same control law $\boldsymbol{u}$ will be applied to each vessel. For the cooperative control the $\boldsymbol{u}$ control law is given by:

$$\boldsymbol{u}_{A,B}=\boldsymbol{K}_P\boldsymbol{e}_{A,B}+\boldsymbol{K}_D\dot{\boldsymbol{e}}_{A,B}+\boldsymbol{K}_I\int\boldsymbol{e}_{A,B}dt+\boldsymbol{K}_c\boldsymbol{e}_c^{A,B} \quad (8)$$

where $\boldsymbol{K}c$ stands for the cooperative "proportional" control gain and $\boldsymbol{e}_c^A=-\boldsymbol{e}_c^B=\Delta\boldsymbol{r}-\Delta\boldsymbol{x}$.

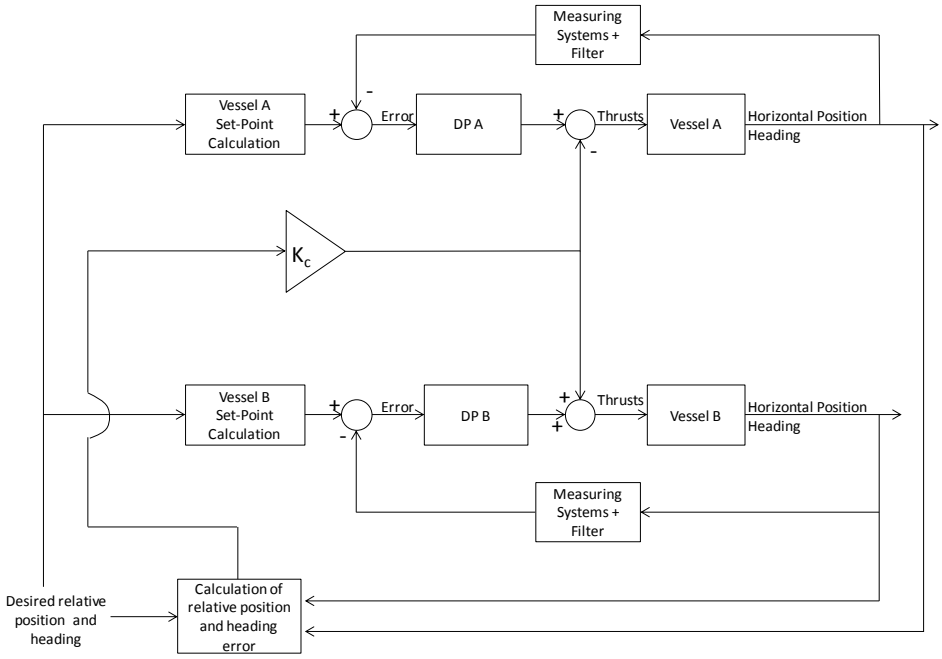

Fig. 4. Cooperative control system.

By replacing eq. (8) in eq. (5) the cooperative closed-loop system stays as:

$$(\boldsymbol{M}+\boldsymbol{M}^{ad})\Delta\ddot{\boldsymbol{x}}+(\boldsymbol{D}+\boldsymbol{K}_D)\Delta\ddot{\boldsymbol{x}}+(\boldsymbol{K}_P+2\boldsymbol{K}_c)\Delta\dot{\boldsymbol{x}}+\boldsymbol{K}_I\Delta\boldsymbol{x}=\boldsymbol{K}_D\Delta\ddot{\boldsymbol{r}}+(\boldsymbol{K}_P+2\boldsymbol{K}_c)\Delta\dot{\boldsymbol{r}}+\boldsymbol{K}_I\Delta\boldsymbol{r}+\Delta\boldsymbol{F}^d \quad (9)$$

Numerical Simulations

All experiments were conducted at the TPN's numerical simulator (more about the TPN's numerical simulator can be found at Nishimoto et al. 2003). The tests were chosen to validate the controller under two different situations: one is to verify the performance of the controller under tracking (set-point step change) and another one was chosen to verify the disturbance rejection of the controller (station keeping). The experiments used two typical offshore tugboats. Theirs properties are indicated at Table **2**.

Table 2. System's parameters description.

Parameter	**Value**
Length overall LOA	80.0 m
Length between perp. LPP	69.3 m
Beam	18.00 m
Maximum Draft	6.50 m
Minimum (Lightship) Draft	4.60 m
Maximum Displacement	7,881 ton

The vessels are equipped with two main thrusters, two tunnel thrusters (one at the bow and one at the stern), and an azimuthal bow thruster. Fig. 5 shows all thrusters' parameters and layout. For this DP layout the PID's gains were automatically adjusted by the TPN's offshore simulator considering it is desired that the time response for each degree of freedom to be same. Table 3 shows the adopted gains.

Table 3. System's parameters description.

i	**K_P**	**K_D**	**K_I**
1	8.5 kN/m	6.6×10^{2} kN/(m/s)	5.5×10^{-2} kN/(m.s)
2	14.7 kN/m	1.1×10^{3} kN/(m/s)	9.5×10^{-2} kN/(m.s)
6	4.65×10^{3} kN.m/rad	3.6×10^{5} N.m/(rad/s)	30 kN.m/(rad.s)

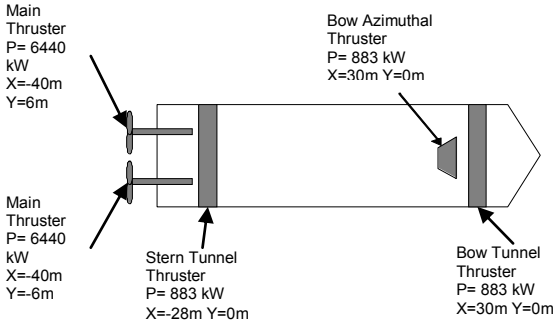

Fig. 5. Tugboat DP layout.

Cooperative control test 1 - tracking performance

In order to verify the controller's tracking performance a set of manoeuvres were carried on the three degrees of freedom, applying a step change in the relative position set-point. A time invariant typical

Campos Basin environmental condition will be considered during the simulation. Fig 6 shows the experiment's adopted layout.

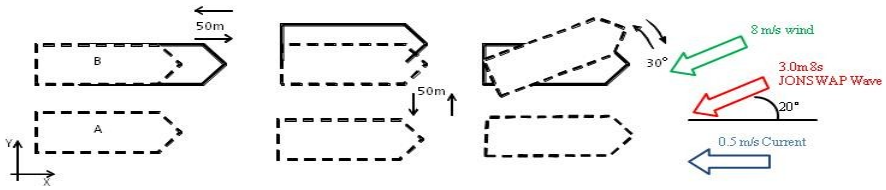

Fig. 6. Maneuvers and incoming environmental conditions (Tracking performance evaluation).

Cooperative control test 2 - Disturbance rejection

In order to verify the controller's ability to reject the disturbances, a set of different environmental conditions will be applied at the system considering a fixed relative distance set-point. At these simulations, the relative distance set-point will be kept unchanged (30° relative heading angle). At this experiment the two tugboats were not positioned parallel to each other. In this case, the magnitude of the disturbances action on the vessels will be significantly different, resulting a large value for the vector Δd_i. The wind and wave direction were changed in intervals of 15° around the two vessels, while the current direction was kept constant. Fig. 7 indicates the experiment layout.

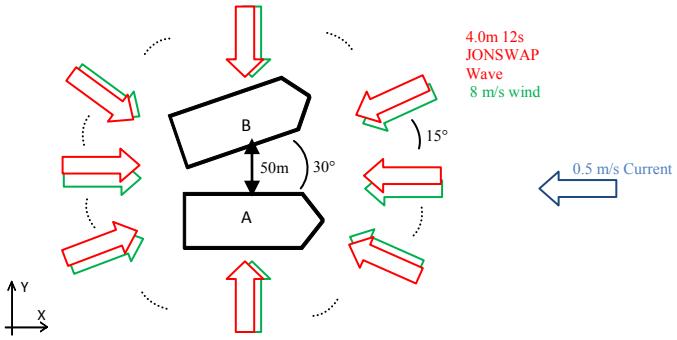

Fig. 7. Incoming environmental conditions (Disturbance rejection evaluation).

Experimental Set-up Description

The experiments were conducted at the Numerical Offshore Tank (USP) (more about the laboratory facilities for DP experiments can be found at Tannuri et. al 2006 and Morishita et. al. 2009). The tests were conducted to validate the controller under various environmental conditions. The experiments used two 1:42 reduced scale model of a typical offshore tugboat, with the full scale properties indicated at Table 4.

Table 4. Model and Full scale tug boat properties

Property	**Model**
Length overall LOA	1.90 m
Length between perp. LPP	1.65 m
Beam	0.43 m
Maximum Draft	0.154 m
Minimum (Lightship) Draft	0.12m
Maximum Displacement	74 kg
Lightship Displacement	50 kg

The lightship condition was used in the tests. The two vessels are equipped with two main thrusters, two tunnel thrusters one in the bow and one in the stern, and an azimuthal thruster which is not going to be considered in this experiment (Fig. 8).

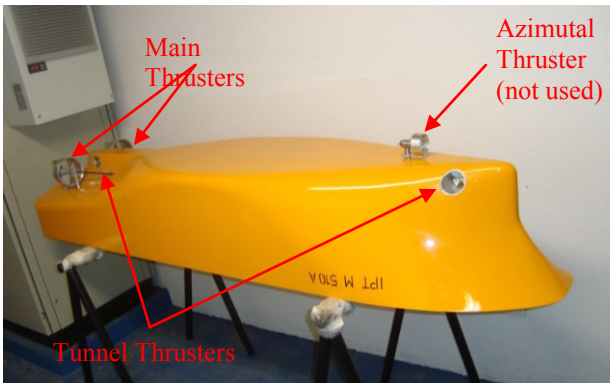

Fig. 8. Model (upside down) and thrusters information.

The tank has a set of fans and a wave generator that produces wind and waves parallel to the tank (Fig. 9). A *Qualisys* measuring system is used for obtaining the horizontal position of both vessels, and the control loop is performed at the scan rate of 100ms.

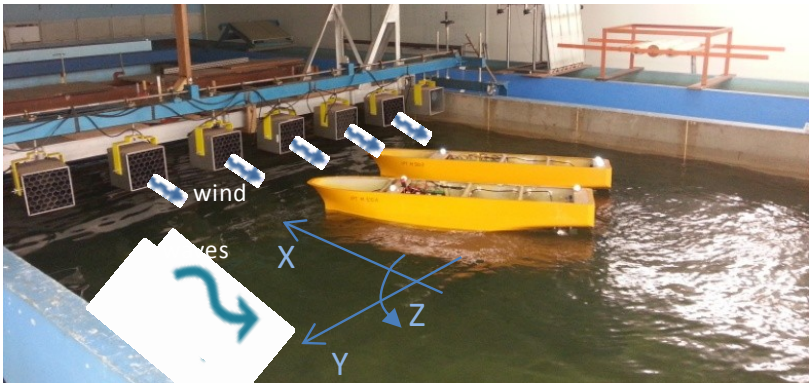

Fig. 9. Models under environmental loadings due to fans aligned with the tank length.

For the experimental tests, all PID gains were empirically adjusted, and the Table 5 shows the obtained values. Both vessel controllers are adjusted with the same gains.

Table 5. K_P, K_D and K_I control gains.

i	**K_P**	**K_D**	**K_I**
1	1.10 N/m	7.57 N.s/m	3.33×10^{-3} N/m.s
2	8.58 N/m	2.08×10^{1} N.s/m	2.00×10^{-2} N/m.s
6	1.24×10^{1} Nm/rad	1.52×10^{1} N.m.s/rad	1.00×10^{-4} Nm/rad.s

Frequency Domain Analysis

Previously to the tests, a frequency domain analysis was performed for both cases: tracking performance and disturbance rejection.

Tracking performance

The following figure (Fig. 10) show the frequency response for the closed loop system in terms of the $\Delta R(s)_1$ system's input and how it is affected by the K_{C_1} gain (surge motion).

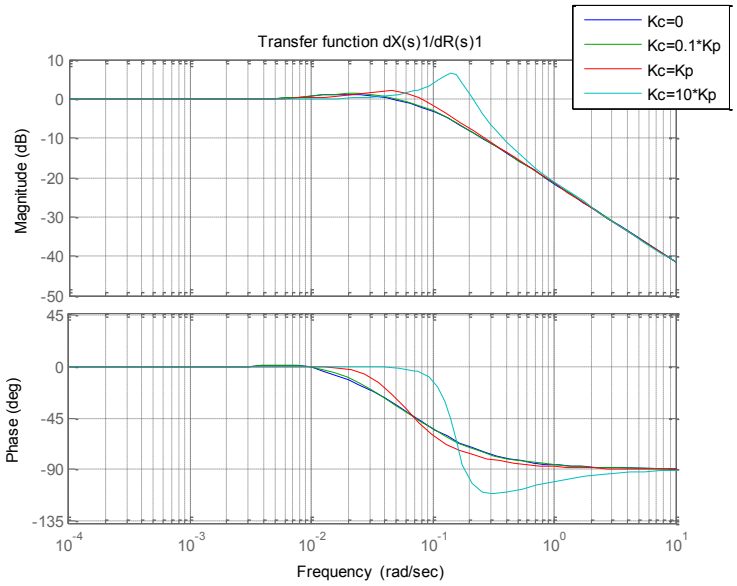

Fig. 10. Bode diagram for $\frac{\Delta X(s)_1}{\Delta R(s)_1}$ for different values of K_{C_1} in terms of K_{P_1}.

As it can be observed, the increase of the K_{C_1} gain enlarges the bandwidth of the system which makes the time response faster. However the total damping of the system is reduced, causing amplification in a frequency range near the natural frequency of the system. This effect is not desirable and imposes an upper limit on the K_{C_1} gain. The same conclusion can be obtained by the analysis of sway and yaw motion transfer functions.

Disturbance rejection

The Fig. 11 shows the frequency response for the closed loop system in terms of the disturbance $\Delta D(s)_1$ and how it is affected by the K_{C_1} gain.

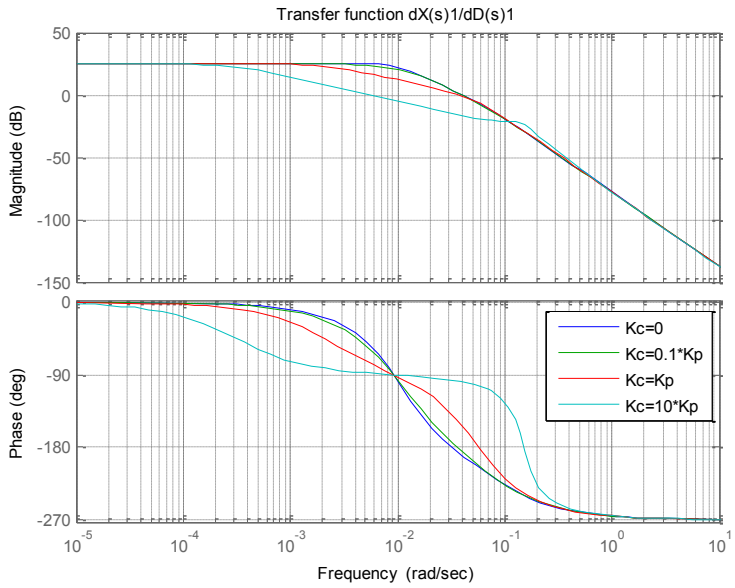

Fig. 11. Bode diagram for $\frac{\Delta X(s)_1}{\Delta D(s)_1}$ for different values of K_{C_1} in terms of K_{P_1}.

As it can be noticed, the increase of the K_{C_1} gain attenuates the system response near the slow drift frequency range in terms of $\Delta D(s)_1$ input, which is a desirable effect since it is wanted that the system rejects the slow drift movement.

ZERO POLE ANALYSIS

Similar to what was done in section 4, a zero-pole analysis was performed for both cases: tracking performance and disturbance rejection. The effects of the $\boldsymbol{K_C}$ gains on the position of the closed-loop zeros and poles will be shown. Since the PID's gains were adjusted such that the poles and zeros of the tree degrees of freedom are placed at the same position on the complex plane, only one zero pole diagram for one degree of freedom (no matter which of them since they are the same) will be shown.

Tracking performance

Fig. 12 shows the Zero Pole diagram for the closed loop system in terms of the $\boldsymbol{\Delta r}$ system's input and how the $\boldsymbol{Kc}$ gain affects it.

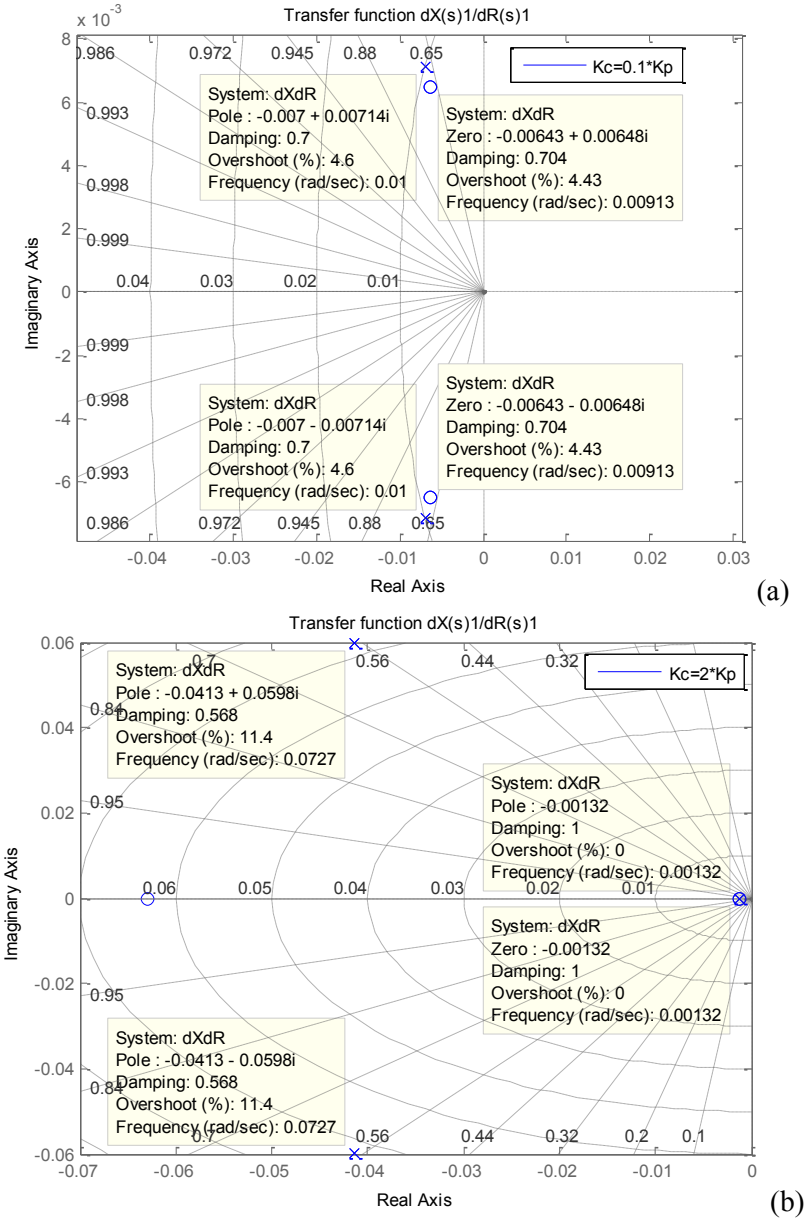

Fig. 12. Zero pole diagram for $\frac{\Delta X(s)}{\Delta R(s)}$; (a) $\mathbf{K_{C_i} = 0.1.K_{p_i}}$; (b) $\mathbf{K_{C_i} = 2.K_{p_i}}$

The increase of the K_C gain brings a zero and a first order pole together near the complex axis cancelling the effect of this pole. The other pair of complex pole, that becomes the dominant one, is removed from its original position into a farthest position which leaves the system's time response faster. The upper limit for the K_C gain is defined by the damping parameter that defines the overshoot and settling time parameters.

Disturbance rejection

Fig. 13 shows the Zero Pole diagram for the closed loop system in terms of the Δd system's input and how it is affected by the K_C gain.

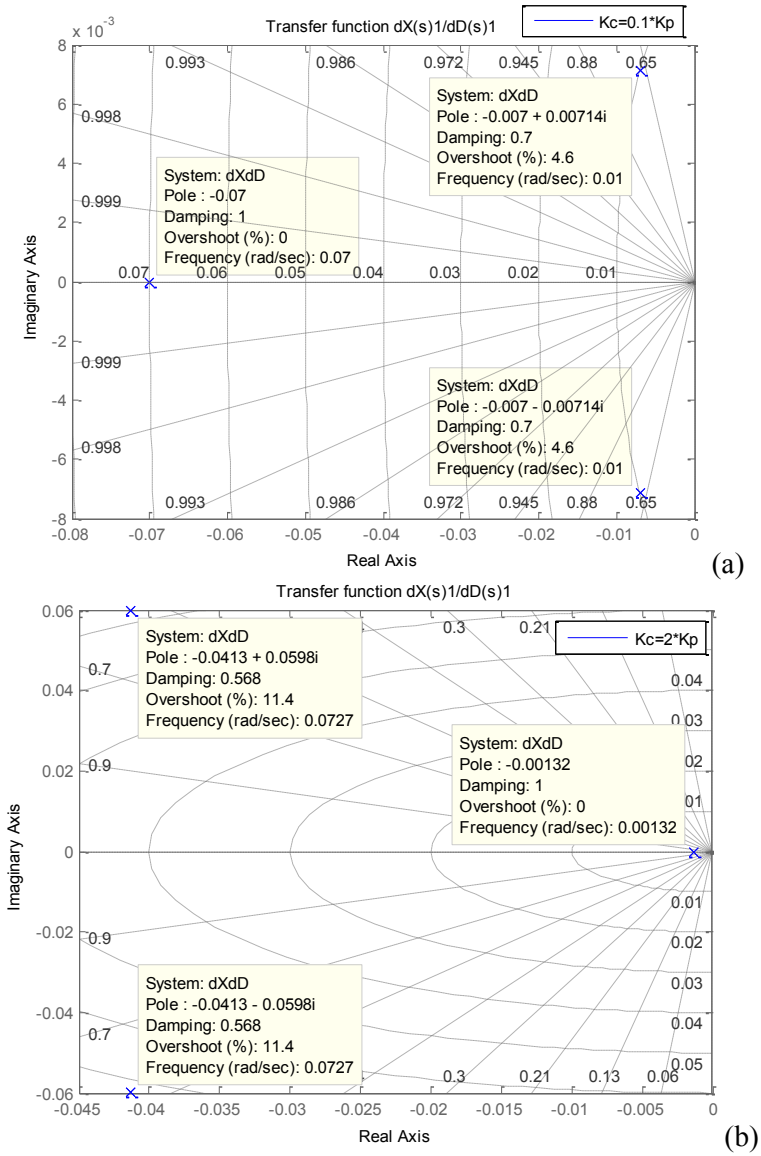

Fig. 13. Dominant zero pole diagram for $\frac{\Delta \mathbf{X(s)}}{\Delta \mathbf{D(s)}}$: (a) $\mathbf{K_{C_i} = 0.1.K_{p_i}}$; (b) $\mathbf{K_{C_i} = 2.K_{p_i}}$

As it can be noticed the increase of the $\boldsymbol{K_C}$ gain brings a first order pole near the complex axis and keep the other pair of complex poles slightly further away. This pole near the complex axis is the dominant pole and let the system's time response slow in terms of $\boldsymbol{\Delta d}$ input which improves the disturbance rejection.

Numerical Simulations

The following simulations were carried on using a modified version of the TPN's numerical simulator which includes the cooperative consensus control. The choice of the $\boldsymbol{K_C}$ gain was made considering a maximum overshoot of 30% which leads approximately to a $\boldsymbol{K_C = 2.K_p}$. Actually an overshoot of 26.8% was expected by the linear analysis presented in the previous section. The closed-loop natural frequency is increased from 0.01 rad/s to 0.0727 rad/s, reducing the settling-time and the rise-time parameters.

Tracking performance

Fig. 14 shows the relative distances between the two tugboats obtained in the numerical simulation. The three step set-point changes (one in each degree of freedom) are also shown. Fig. 15 and Fig. 16 show the vessels A & B thrusters' resultant forces.

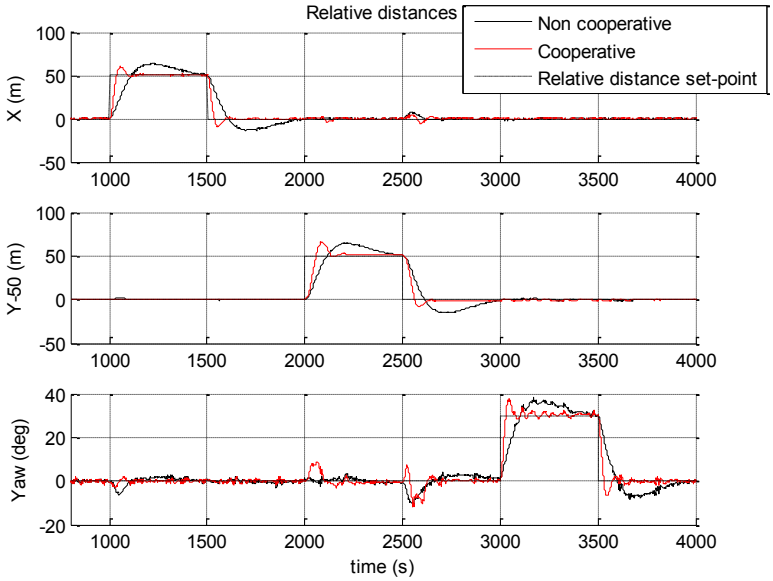

Fig. 14. Relative distances between vessels A & B for cooperative and non-cooperative control system.

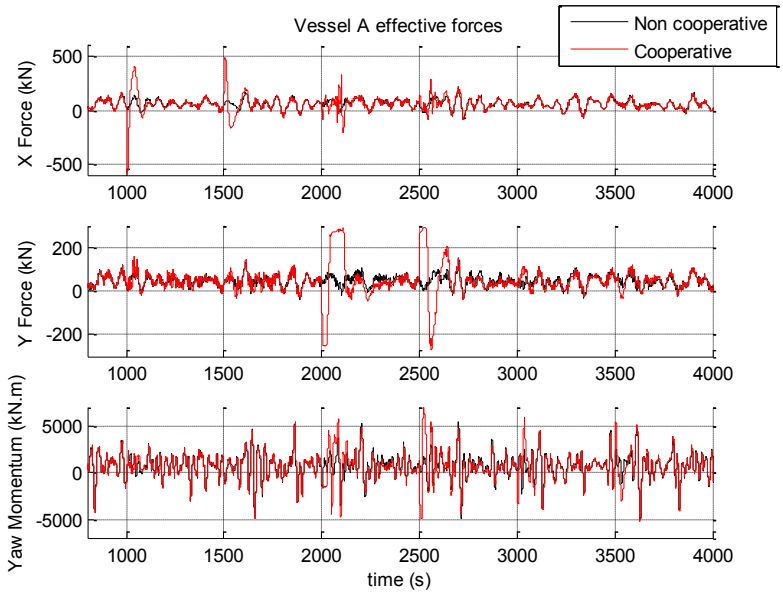

Fig. 15. Vessel A thrusters' resultant forces.

As it can be noticed through Fig. 14, the overall performance is improved when using the cooperative control. In fact Table 6 shows the time-domain performance parameters which confirm the performance improvement. The adoption of $\boldsymbol{Kc} = 2.\boldsymbol{Kp}$ didn't significantly change the overshoot parameter. As

previously stated an overshoot of 26.8% was expected for the cooperative control. Differences in this parameter for surge and sway can be explained through the disturbance incidence (especially for surge where the current incidence is aligned to) and thrusters' saturation during the sway manoeuvre (Fig. 15 and Fig. 16). The rise-time and 5% settling-time are significantly improved when comparing to the standard PID control, showing the benefits of the cooperative control.

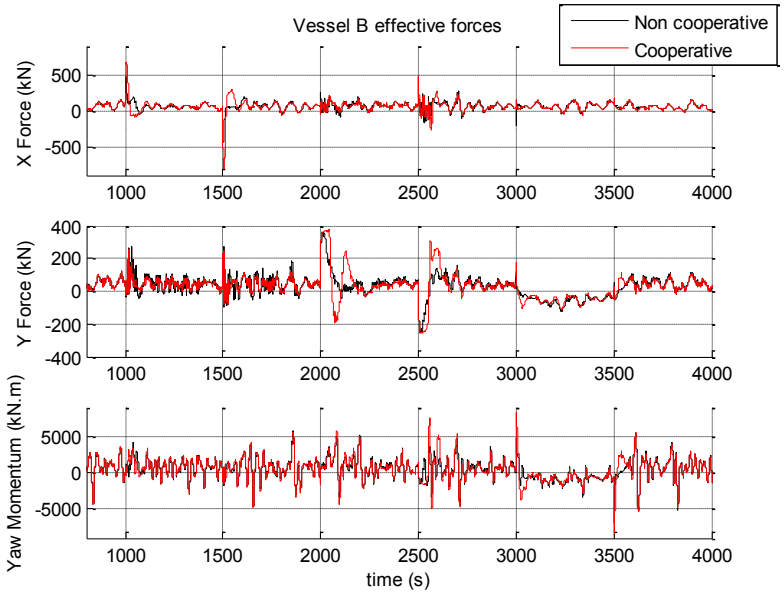

Fig. 16. Vessel B thrusters' resultant forces.

Table 6. Cooperative and non-cooperative overshoot comparison.

	i	Non-cooperative	Cooperative
Overshoot	1	27.2%	20.0%
	2	28.0%	32.0%
	6	27.0%	26.7%
Rise-time	1	67.1s	24.5s
	2	70.3s	41.9s
	6	55.8s	18.6s
5% settling time	1	440.0s	85.5s
	2	450.0s	126.5s
	6	435.0s	230.0s

Disturbance rejection

Fig. 17 show the absolute mean relative distance error for each incidence direction considering a 4.0m significant height and 12s peak period JONSWAP wave, 8m/s wind and 0.5 m/s current.

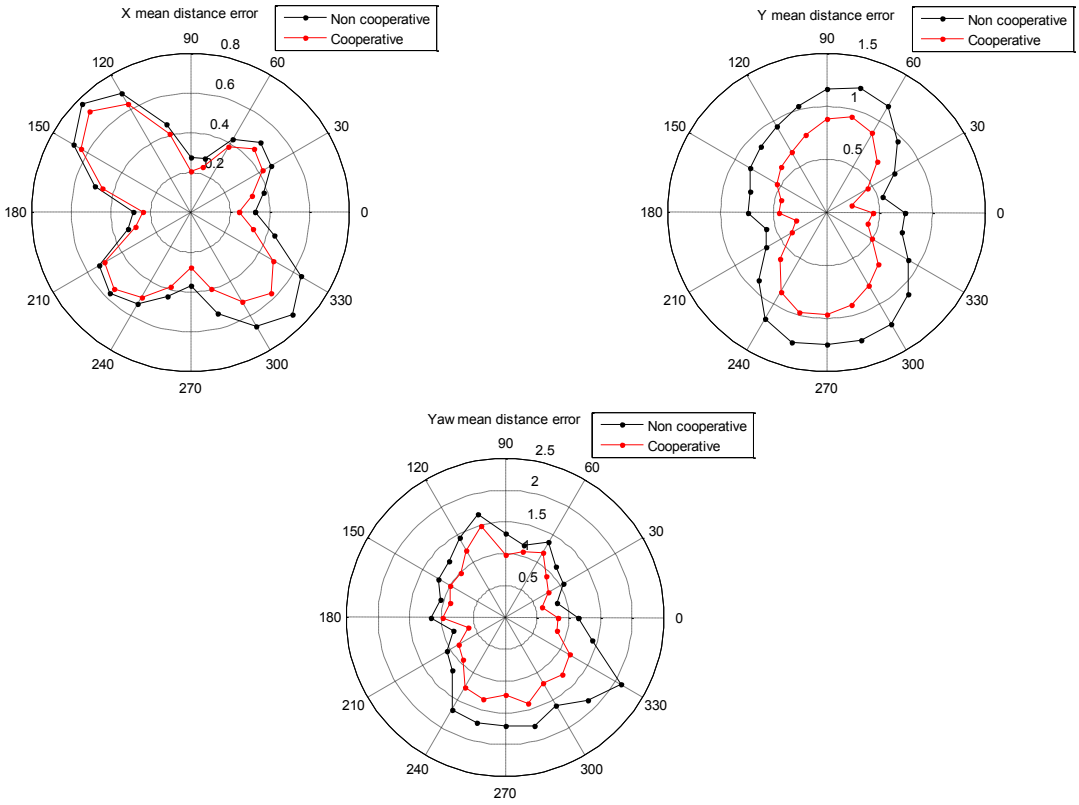

Fig. 17. Absolute mean relative distances for 4.0m significant height and 12s peak period wave, 8 m/s wind and 0.5 m/s current.

As it can be noticed, the overall disturbance rejection is improved when using the cooperative control. In fact the frequency domain analysis showed a gain reduction near the slow drift frequency range (Fig. 11) what is also observed in the numerical tests.

Experimental Results

Non-cooperative control

The first experiment was carried out with non-cooperative control. It aims to show that the PID control gains are well tuned and the performance of the DP positioned vessels is satisfactory for the three degrees of freedom. No environmental action is considered in this test. Negative and positive steps of 0.2m were imposed to surge and sway set-points (Fig. 18). The same kind of manoeuvres was imposed to the yaw angle (10° and 30° step changes).

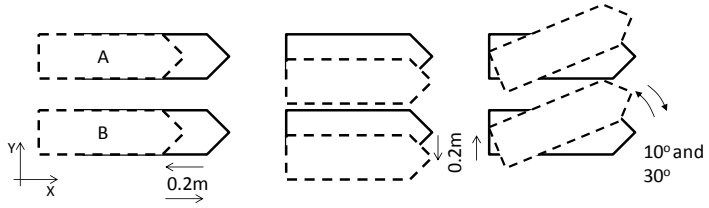

Fig. 18. Vessel A & B Positions (no environmental action).

The experimental results are presented in Fig. 19 (position of both vessels) and Fig. 20 (thrusters' rotation in rpm). As it can be noticed, even with the same PID controller gains, there are significant differences between the performances of the vessels, mainly in sway and yaw directions. It can be explained by some discrepancies in the ballasting arrangements and the propellers mechanical construction and the final rpm-force relation. However, these differences are important to stress the advantages of the cooperative control, as will be discussed in the next section.

The performance is acceptable for the vessels, and the settling time (5% stabilization criteria) and overshoot for the positive degrees are presented in the Table 7.

The thrusters' rotations indicate that the tunnel thrusters get saturated when performing sway and yaw manoeuvres. Since no wave-filter or low-pass filter is being used, some high-frequency oscillation can be detected. However, this behaviour does not affect the comparison between cooperative and non-cooperative control that is the main purpose of the experiments.

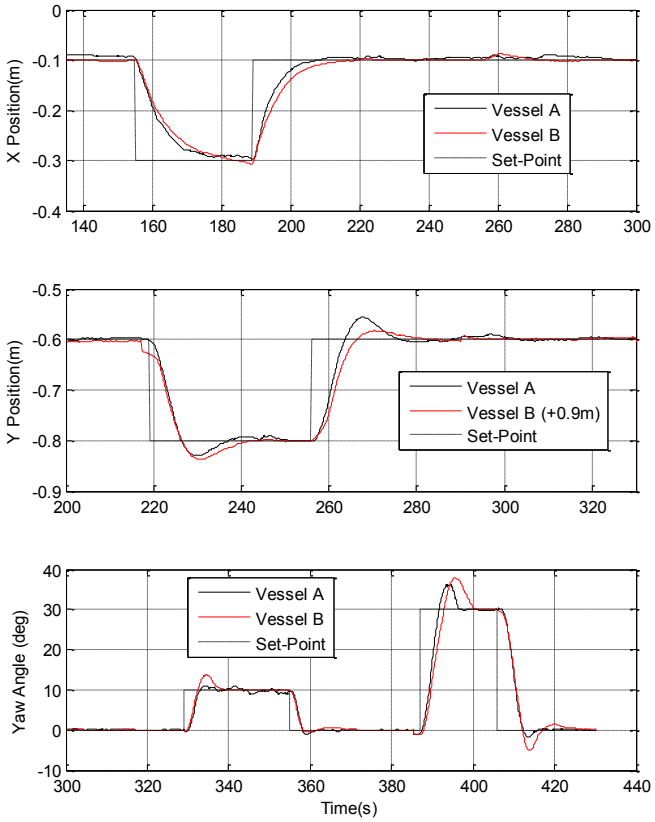

Fig. 19. Vessel A & B Positions (no environmental action).

Table 7. Performance parameters for positive degrees.

	5% Settling Time	**Overshoot**
Surge 0.2m degree	13s (A) ; 19s (B)	2.5% (A) ; 1.5% (B)
Sway 0.2m degree	19s (A) ; 20s (B)	22.0% (A) ; 9.0% (B)
Yaw 30o degree	9s (A) ; 12s (B)	20.0% (S) ; 26.7% (B)

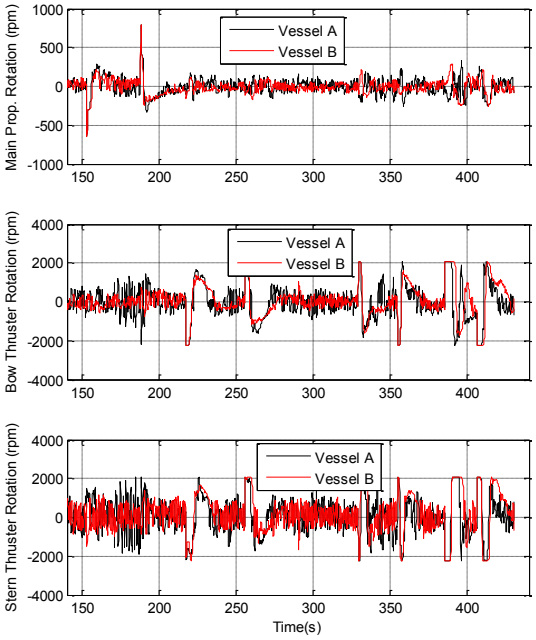

Fig. 20. Main, Bow and Stern thruster's rotation.

Cooperative control - Test 1 - Yaw manoeuvre, no environmental action

The first set of experiments of the cooperative control consists of 4 maneuvers of 30° step set-point change in yaw. Fig. 21 illustrates the experiment. No environmental condition is applied in this test, and the cooperative control gain K_{Cx_6} is varied, in order to illustrate its effects in the overall performance of the vessels. The cooperative control gains K_{Cx_1} and K_{Cx_2} are set to zero in this test.

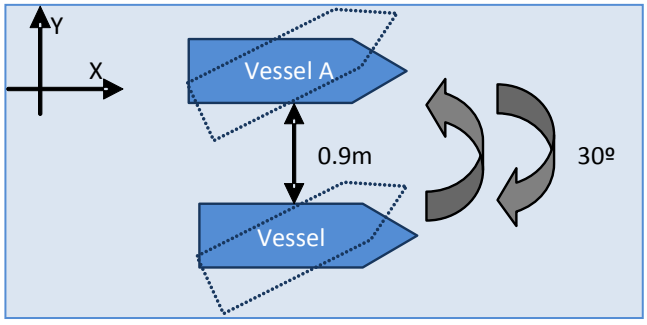

Fig. 21. Maneuvers in yaw.

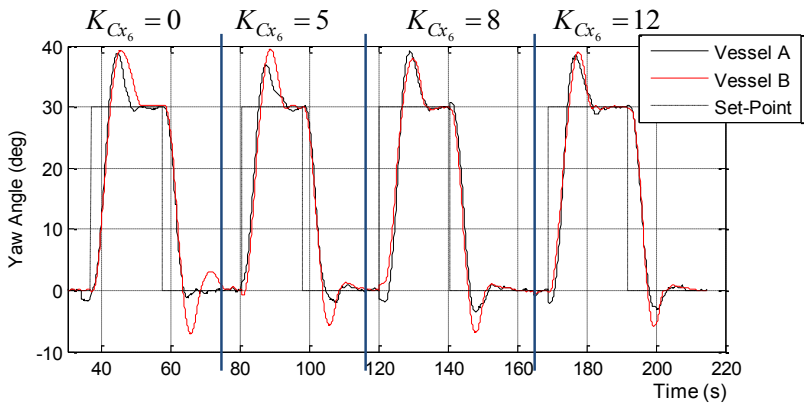

Fig. 22. Vessel A & B Yaw angle for different cooperative control gain values (no environmental action).

As it can be noticed through Fig. 22 the higher is the K_{Cx_6} gain the closer are the two curves during the yaw maneuver. It is an indication of the cooperative control working principle. The Fig. 23 presents the average performance parameters (considering the positive and negative manoeuvres) for the four different K_{Cx_6} gains. It can be verified that the parameters are getting closer when this gain is 8 or 12.

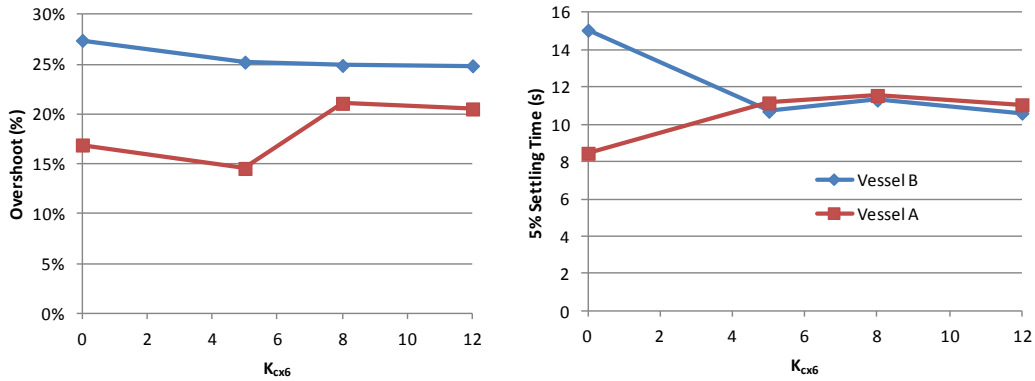

Fig. 23. Performance parameters.

Another important variable of a multiple vessel operation is the distance between them, considering a bow, amidships and stern point of the vessels (Fig. 24). In that figure, a dashed line indicates a rough estimate of the maximum distance variation around the mean value (0.9m). It can be verified the advantage of the cooperative control, that reduces the distance variation from 0.47m to 0.31m (for $K_{Cx_6} = 8$). The cooperative control of the sway motion will reduce this distance variation even more, as will be shown in the next tests.

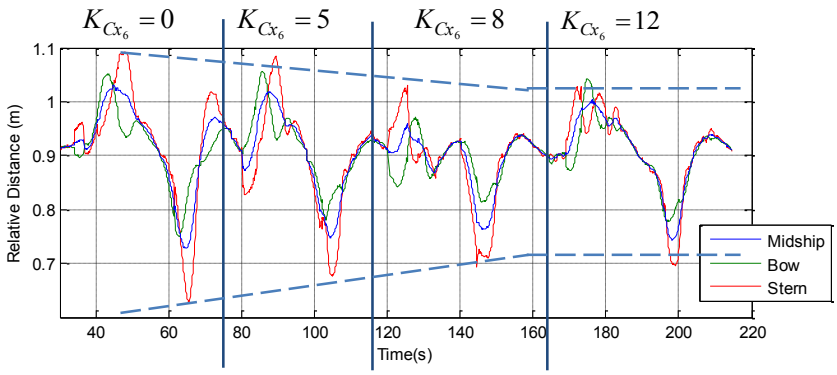

Fig. 24. Distance between different points of the vessels.

The previous results indicated that there was still room to increase the parameter K_{Cx_6} with some improvement in the performance, without loss of stability. So, after some tests, the Fig. 25 shows the final comparison for the 30° yaw manoeuvre, with no cooperative control ($K_{Cx_6} = 0$) and with the final value adopted for yaw cooperative control ($K_{Cx_6} = 15$). Again, the advantages of the cooperative control gets clear, since the yaw motions of the vessels become quite similar.

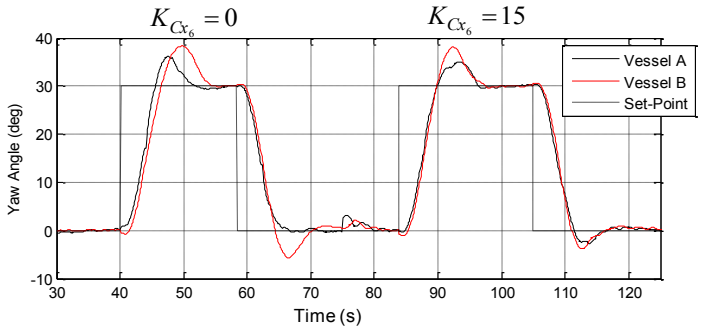

Fig. 25. Vessel A & B Yaw angle for two different cooperative control gain values (no environmental action).

Cooperative control - Test 2 - Sway and Yaw manoeuvres, no environmental action

This set of experiments consists of one manoeuvre of 0.2m step set-point change in sway (Fig. 26) with cooperative control both in yaw and sway axes (K_{Cx_2} = 12 K_{Cx_6}= 15). Another 5 maneuvers of 30 degrees step set-point change in yaw were done varying K_{Cx_2} in order to verify the influence of that parameter in the performance of the controller.

As it can be noticed through Fig. 27 as the K_{Cx_2} gain gets higher the more the both Y position curves get closer. Fig. 28 shows the absolute relative distance error for the amidships point for the whole test. Fig. 29 shows the relative distance mean error for the same point for every pair of value of K_{Cx_2} ($K_{Cx_6} = 15$). It is evident the benefits of the cooperative control for the sway motion also.

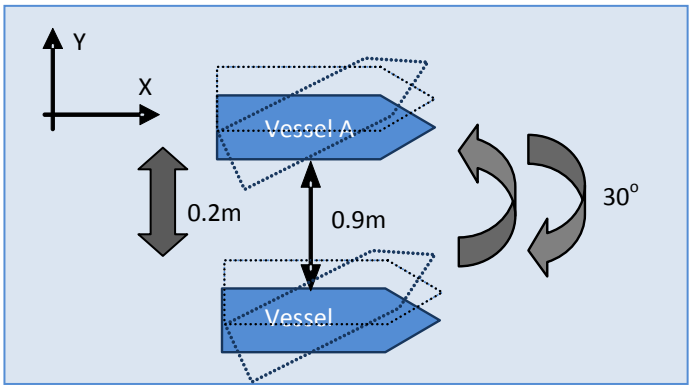

Fig. 26. Maneuvers in sway and yaw.

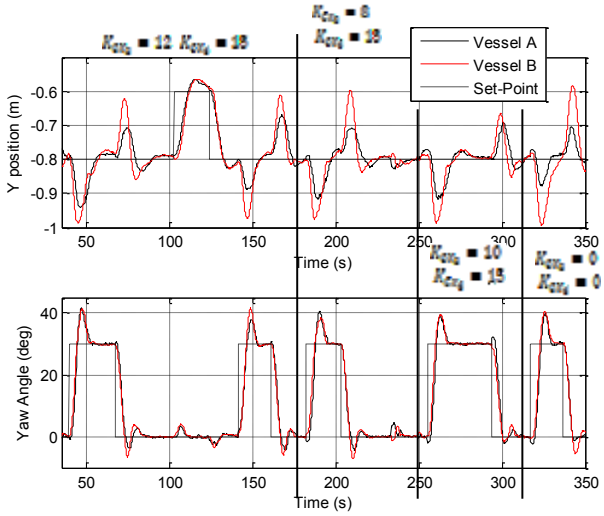

Fig. 27. Vessel A & B sway position and yaw angle for different cooperative control gain values (no environmental action).

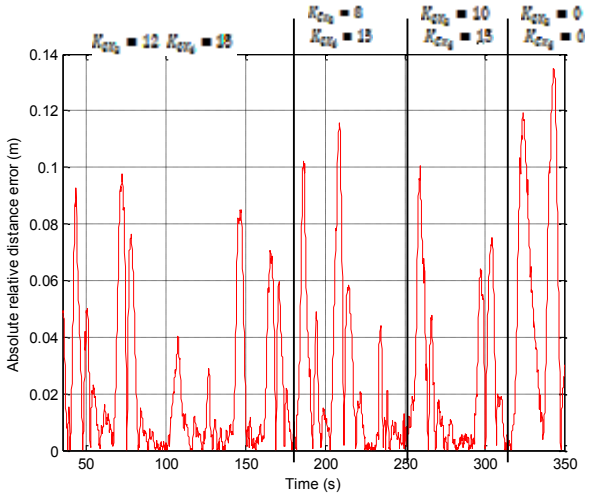

Fig. 28. Absolute relative distance error for different values of the cooperative control gain (no environmental action).

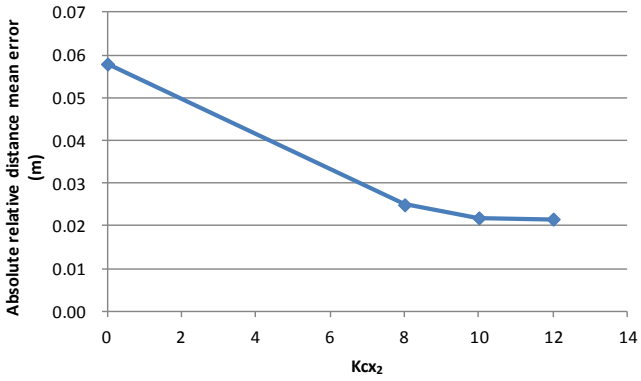

Fig. 29. Absolute relative distance mean error for different values of the cooperative control gain (no environmental action).

Cooperative control - Test 3 - Sway and Yaw maneuvers, with environmental action

This set of experiments consists of maneuvers of 0.2m step set-point change in sway and maneuvers of 30 degrees step set-point change in yaw. Non cooperative control (K_{Cx_2} = 0; K_{Cx_6}= 0) was applied for some tests and cooperative control to others (K_{Cx_2} = 10; K_{Cx_6}= 15). Fig. 30 shows the layout used in the experiments.

Wind and wave actions were considered during these experiments. The wind speed is roughly adjusted to 4m/s (25m/s in full scale). The wave height is approximately 0.1m (4.2m full scale) and 1s period (6.5s full scale). Although no accurate calibration method was used for defining or measuring those values, they indicate that the conditions are strong and feasible in offshore fields. As a reference, the 1-year typical NE condition in Campos Basin (Brazil) presents a 4.5m wave (5s period), with 19m/s wind. The idea is simply to impose some disturbance to the vessels in order to verify the controller behavior.

Fig. 31 shows the Y position and the yaw angle of both vessels. As it can be noticed when the cooperative control is turned off (from 240s until 390s), both position curves (Y and yaw) get apart from each other. In fact, Fig. 32 shows the relative distance between amidships, bow and stern points. At 240s when the cooperative control is turned off the relative distances errors get significantly higher.

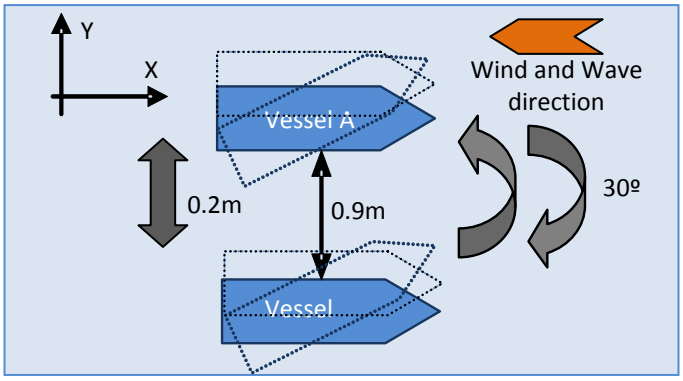

Fig. 30. Maneuvers in sway and yaw with environmental action.

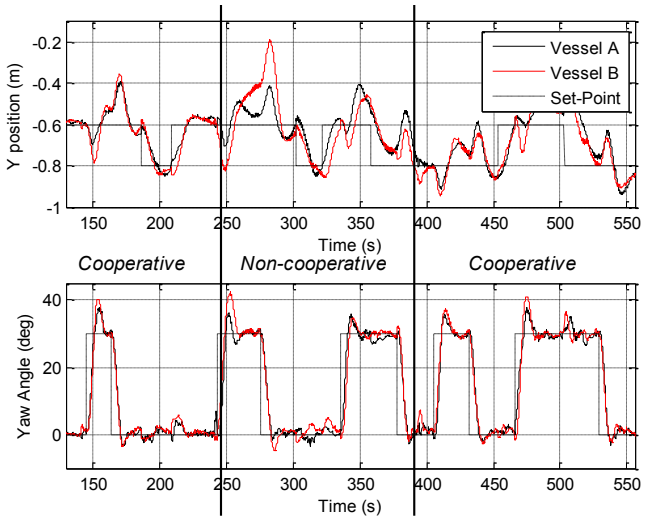

Fig. 31. Vessel A & B Sway position and Yaw angle with environmental action.

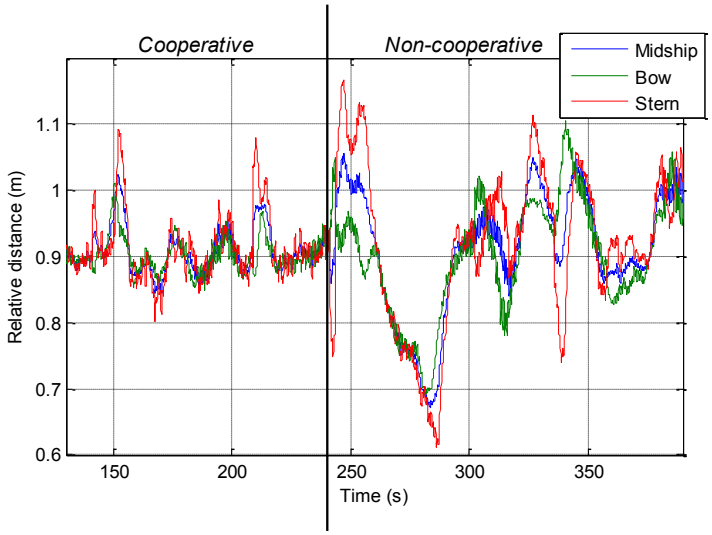

Fig. 32. Relative distance from Keel amidships, bow and stern between the vessels for cooperative and non-cooperative control.

The amidships relative distance mean error calculated for the cooperative and the non-cooperative control are respectively 2.41×10^{-2}m and 7.17×10^{-2}m. An improvement of approximately 3 times is verified using the cooperative control.

Conclusion

This paper presented the application of a cooperative control based on the consensus concept applied to coordinated manoeuvres. The concept of cooperation control applied to DP operations is innovative and can be extended to different types of operations that require multiple vessels, such as ship to ship oil or fuel transfer.

Numerical tests showed that the tracking performance and disturbance rejection of the relative distance were improved when compared to the standard DP control. The time-domain performance parameters of

the system such as the rise-time and settle-time were reduced without significantly changes on the overshoot parameter. Also the relative distance between the ships varied less when using the cooperative control. Two tugboats were used in the experiments. Small scale tests also obtained the same results when using the cooperative control. Two scale model tugboats were used in the experiments.

For a matter of comparison Fig. 33 shows the yaw position for vessels A & B during a 30° yaw step step-point change for the standard DP control (left) and for the cooperative control (right), for the small scale experiment. It is observable that the cooperative control approximates both curves.

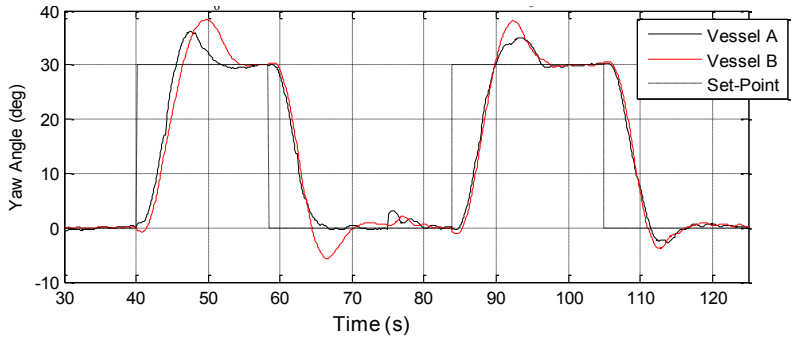

Fig. 33. Vessels A & B yaw position for non-cooperative control (left) and for the cooperative control (right) during the small scale experiment.

The same manoeuvre was performed numerically, using the modified TPN simulator and the used tugboats' models in the tests. Fig. 34 shows the result.

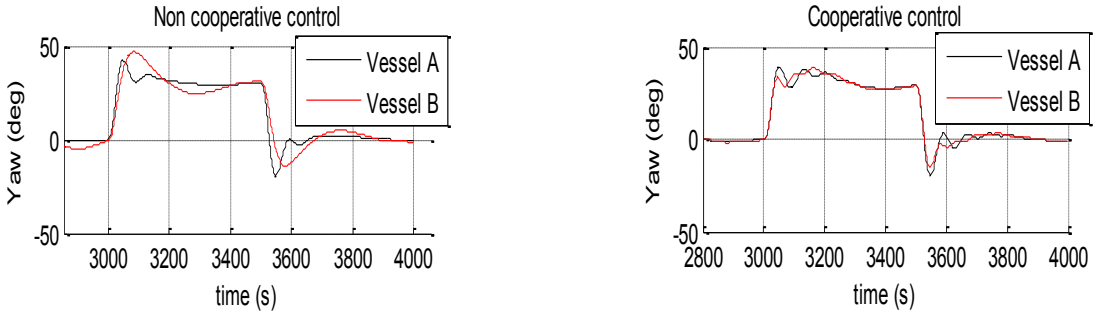

Fig. 34. Vessels' A & B yaw position for non-cooperative control (left) and for the cooperative control (right) during numerical experiment.

The same behavior is observed on the numerical experiment reinforcing the advantages of the cooperative control, since the yaw motions of the vessels become quite similar when using the cooperative control. In other words this is the reduction of the relative distance error provided by the cooperative control.

Acknowledgements

The authors would like to thank the National Council for Scientific and Technological Development CNPq (process 302544/2010-0), CAPES for the research grant, Brazilian Innovation Agency FINEP (01.10.0748.00) and São Paulo Research Foundation - FAPESP (2010/15348-4) for sponsoring this research. The authors also thank Petrobras for the constant support for DP research projects and for the initial motivation of this work.

References

Fujarra, A. L. C., Tannuri, E. A., Masetti, I. Q., Igreja, H. **Experimental and Numerical Evaluation of the Installation of Sub-Sea Equipments for Risers Support.** In: 27th International Conference on Offshore Mechanics and Arctic Engineering (OMAE2008), Estoril, Portugal, 2008.

Morishita, H.M. ; Tannuri, E. A. ; Saad, A. C. ; Sphaier, S. H. ; Lago, G.A. ; Moratelli JR., L. **Laboratory Facilities for Dynamic Positioning System.** In: 8th Conference on Maneuvering and Control of Marine Craft, MCMC 2009, Guarujá, Brazil, 2009.

Nishimoto, K. et al. (2003). **Numerical Offshore Tank: Development of Numerical Offshore Tank for Ultra Deep Water Oil Production Systems.** In: 22nd International Conference on Offshore Mechanics & Arctic Engineering (OMAE 2003), June, Cancun Mexico 2003.

Queiroz Filho, A. N. ; Tannuri, E. A. ; Da Cruz, J. J., **A Shuttle Tanker Position Cooperative Control Applied to Oil Transfer Operations Based on the LQG/LTR Method. In: 9th Conference on Maneuvering and Control of Marine Craft**. MCMC 2012, Arenzano, Italy, 2012.

Ren, W.; Beard, R.W.; Atkins, E.M., **Information Consensus in Multivehicle Cooperative Control, IEEE Control Systems Magazine,** April, 2007.

Tannuri, E.A.; Morishita, H.M. **Experimental and Numerical Evaluation of a Typical Dynamic Positioning System.** Applied Ocean Research, v. 28, p. 133-146, 2006.